# Activity and characterization by XPS, HR-TEM, Raman spectroscopy, and bet surface area of CuO/CeO2-TiO2 catalysts

**ARTICLE** *in* THE JOURNAL OF PHYSICAL CHEMISTRY B · NOVEMBER 2001

Impact Factor: 3.3 · DOI: 10.1021/jp0109675



**5 AUTHORS**, INCLUDING:

Valmor R Mastelaro
University of São Paulo
**173** PUBLICATIONS **2,222** CITATIONS

SEE PROFILE

Pedro Nascente
Universidade Federal de São Carlos
**132** PUBLICATIONS **1,648** CITATIONS

SEE PROFILE

# Activity and Characterization by XPS, HR-TEM, Raman Spectroscopy, and BET Surface Area of $CuO/CeO_2$-$TiO_2$ Catalysts

**Maria Suzana P. Francisco and Valmor R. Mastelaro***

*Departamento de Física e Ciência dos Materiais, Instituto de Física de São Carlos, Universidade de São Paulo, C. P. 369, São Carlos, SP, Brazil 13560-970*

**Pedro A. P. Nascente**

*Centro de Caracterização e Desenvolvimento de Materiais, Departamento de Engenharia de Materiais, Universidade Federal de São Carlos, São Carlos, SP, Brazil 13565-905*

**Ariovaldo O. Florentino**

*Departamento de Química, Instituto de Biociências, Universidade Estadual Paulista, Botucatu, SP, Brazil 18618-000*

*Received: March 15, 2001; In Final Form: July 14, 2001*

Structural and textural studies of a $CuO/TiO_2$ system modified by cerium oxide were conducted using Raman spectroscopy, transmission electron microscopy (TEM), X-ray photoelectron spectroscopy (XPS), and $N_2$ absorption (BET specific surface area). The introduction of a minor amount of $CeO_2$ ($Ce_{0.09}Ti_{0.82}O_{1.91}Cu_{0.09}$ sample) resulted in a material with the maximum surface area value. The results of Raman spectroscopy revealed the presence of only two crystalline phases, $TiO_2$ anatase and $CeO_2$ cerianite, with well-dispersed copper species. TEM micrographs showed a trend toward smaller $TiO_2$ crystallites when the cerium oxide content was increased. The XPS analysis indicated the rise of a second peak in Ti 2p spectra with the increasing amount of $CeO_2$ located at higher binding energies than that due to the $Ti^{4+}$ in a tetragonal symmetry. The $CuO/TiO_2$ system modified by $CeO_2$ displayed a superior performance for methanol dehydrogenation than the copper catalyst supported only on $TiO_2$ or $CeO_2$.

## Introduction

Previous studies have shown that there are many applications for $CuO/TiO_2$ material in the field of heterogeneous catalysis, mainly as oxidation catalysts.[1−5] However, this system presents several disadvantages such as thermal and mechanical instabilities, sintering of both the supports, and the active and titania phase transformation.[6,7] Stabilizing a material to avoid these effects can usually be achieved by changing its bulk or surface composition. It has been reported that $CeO_2$ has the property of stabilizing not only the active phase in a fine dispersed state and the resistance to thermal loss of the supported catalyst surface area but also the catalytic activity.[6,8]

The dispersing effect of $CeO_2$ and the synergistic effect between CuO and $CeO_2$ in the combustion of CO and methane have been observed in the Cu−Ce−O system.[9,10] $CeO_2$ promotes the hydrogen reduction of finely dispersed CuO surface species at low temperatures.[11] Alves et al. have studied the effect of the addition of $CeO_2$ in the $IrO_2/TiO_2$ system that is employed as an electrocatalyst.[12] They found that ceria did not form a solid solution with either $IrO_2$ or $TiO_2$ and that its action was confined to that of a dispersing agent, resulting in a higher active surface area. The effects of the addition of $CeO_2$ on the Co−$SiO_2$ catalyst have been investigated, and the results have demonstrated that surface cobalt is more readily reduced in the presence of ceria and that ceria was well dispersed on the silica support.[13]

Oxidative processes in catalysis are most commonly used to obtain products with a high commercial value from molecules with low aggregate value.[7,14] Methyl formate is an attractive intermediate in the production of numerous chemicals, such as formic acid, dimethyl formamide, acetic acid, formamide, and cyanhydric acid. A very well-known process to obtain methyl formate is by methanol dehydrogenation on copper-supported catalysts, which shows high catalytic activity and selectivity.[2]

The present work is an extension of our earlier structural studies of the $CuO/TiO_2$ system modified by cerium oxide.[15] We investigated the catalytic performance of our samples with regard to methanol oxidation. Moreover, structural information was obtained through TEM, Raman spectroscopy, and XPS techniques. The specific surface area was obtained with the purpose of investigating the textural properties, after which the structural and textural results were compared. The overall findings were then correlated with the synergistic effect between copper and $CeO_2$−$TiO_2$ for methanol dehydrogenation.

## Experimental Procedures

**Preparation Synthesis.** Titania-based mixed oxides were prepared by the sol−gel method. Commercial $(NH_4)_2Ce(NO_3)_6$ powder (Vetec) was dissolved in an aqueous nitric acid solution (1.5 mol/L). The $Cu(NO_3)_2{\cdot}3H_2O$ powder (Vetec) was then added, heated to 353 K, and kept at this temperature for 30 min. The resulting solution was dubbed A. Another solution, dubbed B, was prepared with tetraisopropyl orthotitanate ($C_{12}H_{28}O_4TiO$, Merck), which was dissolved in isopropyl alcohol (mole ratio = 1). Solution A was added to solution B

* To whom correspondence should be addressed. Phone: 55-16-2739828. Fax: 55-16-2713616. E-mail: valmor@if.sc.usp.br.

10.1021/jp0109675 CCC: $20.00 
Published on Web 10/09/2001

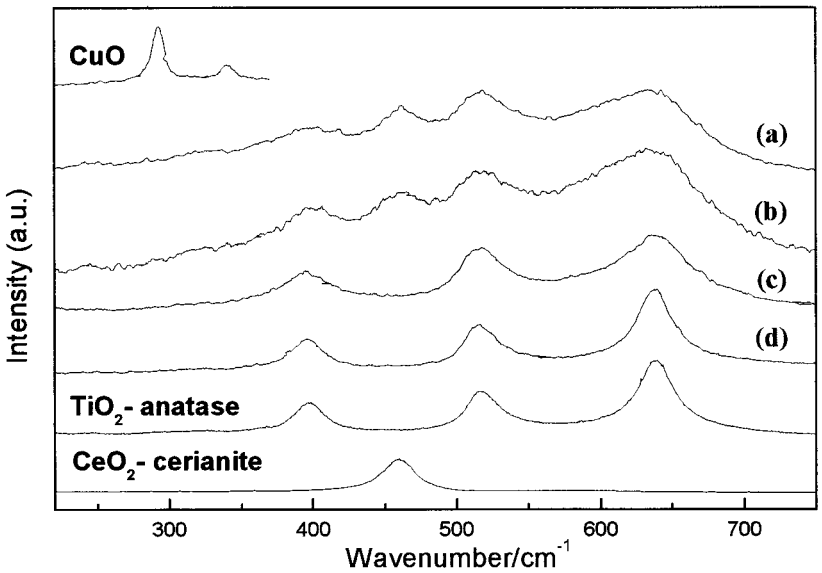


**Figure 1.** FT-Raman spetra of samples: (a) $Ce_{0.45}Ti_{0.46}O_{1.91}Cu_{0.09}$, (b)$Ce_{0.27}Ti_{0.64}O_{1.91}Cu_{0.09}$, (c) $Ce_{0.09}Ti_{0.82}O_{1.91}Cu_{0.09}$, and (d) $Ti_{0.91}O_{1.91}Cu_{0.09}$.

and subjected to a 50 W ultrasonic vibration for 2 min. The mixture was allowed to rest for 24 h in a saturated atmosphere of isopropyl alcohol. Finally, the resulting gel was dried at 383 K for 16 h and then calcined at 723 K for 16 h in air. The prepared powder $CuO-CeO_2/TiO_2$ samples, called $Ce_{0.91}O_{1.91}Cu_{0.09}$, $Ti_{0.91}O_{1.91}Cu_{0.09}$, $Ce_{0.09}Ti_{0.82}O_{1.91}Cu_{0.09}$, $Ce_{0.27}Ti_{0.64}O_{1.91}Cu_{0.09}$, and $Ce_{0.45}Ti_{0.46}O_{1.91}Cu_{0.09}$, express the amount of each component as atomic fractions. $TiO_2$ and $CeO_2$ were used as structural references.

**Characterization.** The specific surface area (BET) was measured with a Micromeritics AccuSorb 2100E instrument, using the adsorption of $N_2$ at the temperature of liquid nitrogen. Prior to measuring, all of the samples were degassed at 523 K for 16 h and finally outgassed to $10^{-3}$ Torr.

Raman spectra were recorded on a triple Jobin-Yvon T64000 Raman instrument equipped with a microscope and a CCD detection system. The spectra were obtained at room temperature using the 5145 Å line of an argon ion laser (model Spectra Physics 2020) excited with an incident power of 50 mW.

An analysis was made using HR-TEM (high-resolution transmission electron microscopy) at 300 kV on a JEOL JEM-3010 microscope from the Laboratory of Electronic Microscopy at the National Sinchrotron Light Source Laboratory in Campinas, Brazil, with a point resolution of 0.17 nm. The powder was ultrasonically suspended in isopropyl alcohol, and the suspension was deposited on a copper grid previously covered with a thin layer of carbon.

An XPS analysis was performed in an ultrahigh vacuum (low $10^{-7}$ Pa range) using a Kratos XSAM HS spectrometer, with a Mg K$\alpha$ ($h\nu = 1253.6$ eV) X-ray source operated at 15 kV and 15 mA. The powder samples were fixed on a steel holder with double-face adhesive tape and analyzed as received. An electron flood gun was used to reduce charge effects. The high-resolution spectra were obtained with an analyzer pass energy of 20 eV. The binding energies were referenced to an adventitious carbon 1s line set at 284.8 eV. Gaussian line shapes were used to fit the curves for C 1s, O 1s, and N 1s, and a mixed Gaussian/Lorentzian function was employed for Cu 2p, Ti 2p, and Ce 3d. The Shirley background and a least-squares routine were applied. The sensitivity factors for quantitative analysis were referenced to $S_{F1s} = 1.0$.

**Catalytic Experiments.** Methanol oxidation was carried out in a fixed bed reactor working under atmospheric pressure and in a temperature range of 443−583 K under steady-state conditions. The temperature was measured by a K-type thermocouple located just above the catalyst bed. A catalyst load of 150 mg was used in each experiment. The methanol was fed into the reactor by bubbling a flow of nitrogen (50 $cm^3$/min) through a saturator−condenser maintained at 305 K, which supplied a constant methanol concentration of 11.6% vol. during the run. An on-line Shimadzu gas chromatograph GC-14B using Supel-Q and Carboxen-1010 Plot capillary columns was used to analyze all of the products. The absence of a homogeneous combustion of reactants and products at temperatures up to 623 K was confirmed by using powdered Pyrex glass. The catalyst was pretreatment-activated with 300 $cm^3$ $h^{-1}$ of flowing 7% $H_2$ and Ar as inert gas at 653 K for 1 h.

**TABLE 1: Specific Surface Area and Titania Crystallite Sizes Obtained through TEM Micrographs**

| samples | $S_{BET}$ ($m^2$ $g^{-1}$) | crystallite sizes of $TiO_2$ [$t \pm 10\%$ (nm)] |
|---|---|---|
| $CeO_2$ | 25 | |
| $TiO_2$ | 79 | 17 |
| $Ti_{0.91}O_{1.91}Cu_{0.09}$ | 84 | 17 |
| $Ce_{0.09}Ti_{0.82}O_{1.91}Cu_{0.09}$ | 124 | 13 |
| $Ce_{0.27}Ti_{0.64}O_{1.91}Cu_{0.09}$ | 105 | 7 |
| $Ce_{0.45}Ti_{0.46}O_{1.91}Cu_{0.09}$ | 80 | 5 |

## Results and Discussion

**Specific Surface Area ($S_{BET}$) − $N_2$ Adsorption.** The specific surface area ($S_{BET}$) for $TiO_2$/CuO showed a clear dependence on added ceria, as shown in Table 1. The $TiO_2$ anatase phase and the $Ti_{0.91}O_{1.91}Cu_{0.09}$ catalyst sample presented approximately the same value of $S_{BET}$ (79 and 84 $m^2$/g, respectively), indicating no influence of copper on the titania surface area. A 9% addition of $CeO_2$ to the $Ti_{0.91}O_{1.91}Cu_{0.09}$ sample ($Ce_{0.09}Ti_{0.82}O_{1.91}Cu_{0.09}$ catalyst) led to a considerable increase of the surface area, i.e., 124 $m^2$/g. The BET area of samples containing greater amounts of $CeO_2$ (27, 45, and 41%, respectively) decreased (105, 80, and 86 $m^2$/g, respectively). In fact, the cerium oxide phase presented the lowest surface area, 25 $m^2$/g.

According to Yuan et al.,[16] the addition of potassium to the $CuO/TiO_2$ system prevented titania sintering, increased the specific surface area of the oxides, and improved the catalytic

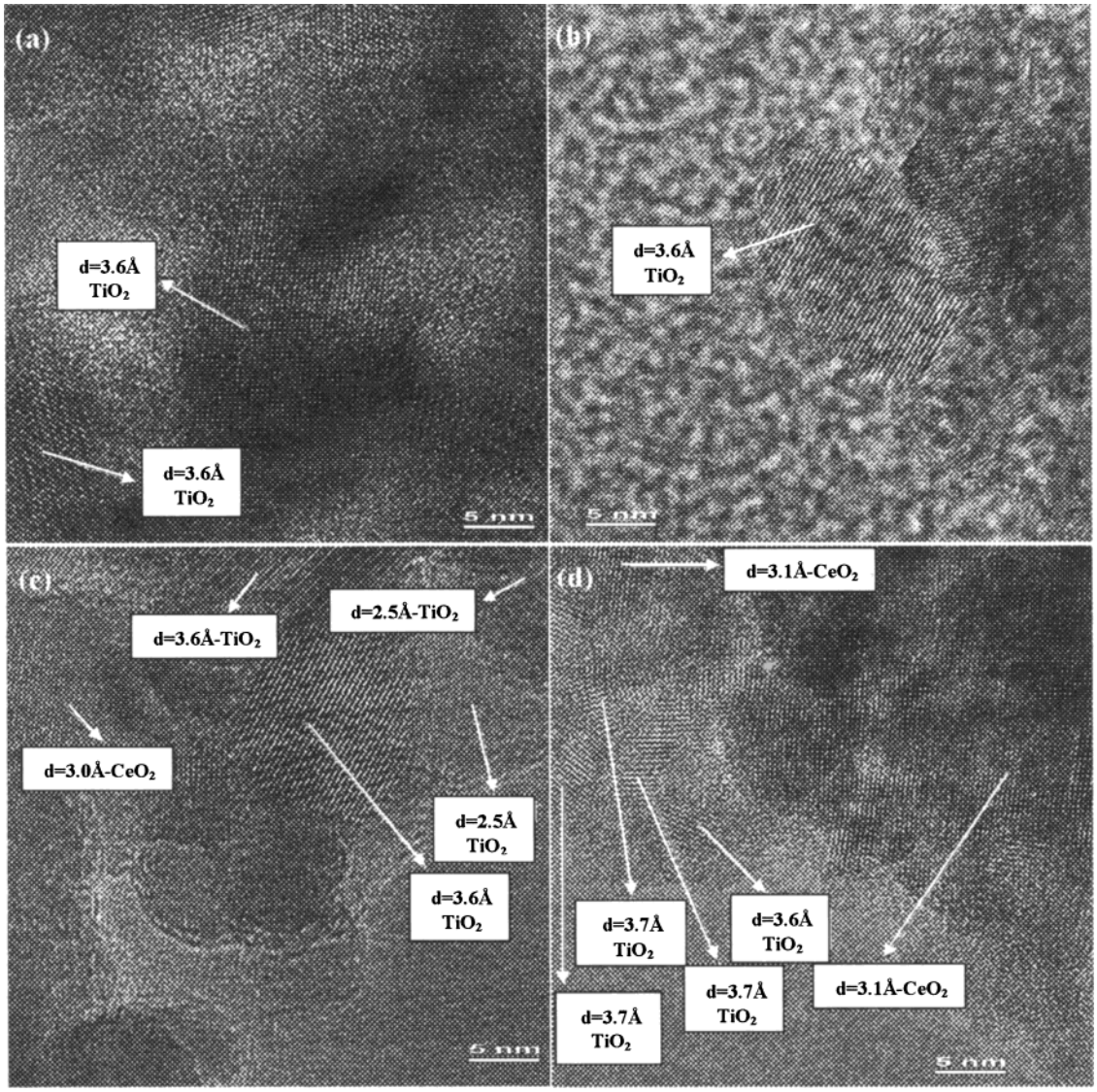


**Figure 2.** TEM micrographs of (a) $TiO_2$, (b) $Ti_{0.91}O_{1.91}Cu_{0.09}$, (c) $Ce_{0.09}Ti_{0.82}O_{1.91}Cu_{0.09}$, and (d) $Ce_{0.45}Ti_{0.46}O_{1.91}Cu_{0.09}$.

performance. Titania modified with 3 and 12 $\mu$mol Ce/m$^2$ surface area of the titania (173 m$^2$/g) were prepared and used as supports for copper oxides.[6] $CeO_2$ added to the $CuO/TiO_2$ system stabilized the surface area of the $TiO_2$ support in the presence of copper oxide.[6]

**Raman Spectroscopy.** Figure 1 shows the Raman spectra after $CeO_2$ loading in the $CuO/TiO_2$ catalytic system. The $TiO_2$ powder phase is known to have well-defined Raman scattering bands[17,18] which, as shown in our results in Figure 1, is easily detected by the intense Raman bands at 397, 517, and 637 cm$^{-1}$ and is in good agreement with previous manuscripts.[6,17−19] For the $CeO_2$ compound, the strong typical band at 460 cm$^{-1}$ is due to the Raman active mode characteristic of fluorite-structured materials.[6,20] The CuO compound presented the strongest band at 293 cm$^{-1}$, a position similar to that reported by other authors.[6,21] Figure 1 shows the Raman spectra after $CeO_2$ loading in the $CuO/TiO_2$ catalytic system.

The catalyst spectra showed only the $TiO_2$ and $CeO_2$ bands. The Raman bands of $CeO_2$ were only observed in the spectra of samples of the $Ce_{0.27}Ti_{0.64}O_{1.91}Cu_{0.09}$ composition (Figure 1a,b). The Raman bands of $TiO_2$ appeared in all of the catalyst spectra, although their intensity was lower than that of the ceria band in samples containing higher amounts of $CeO_2$.

The fact that the Raman spectra exhibited no detectable CuO bands is an indication that CuO was well dispersed in the support structure. This state is in agreement with previous XRD analyses, which presented no X-ray reflection relating to the CuO phase, even in the sample with a higher Cu/(Ti + Ce) ratio (0.22), the $Ce_{0.41}Ti_{0.41}O_{1.82}Cu_{0.18}$ sample.[15] According to the literature, the preparation method and the addition of new components to the support have significant effects on the catalytic properties.[6,22] Thus, the introduction of $CeO_2$ promoted the formation of a material with favorable textural properties.

The formation of a CuO bulk phase in the Cu−Ce(La)−O catalyst system was only observed in samples containing a high amount of copper.[9] From their studies of CuO supported on $CeO_2-Al_2O_3$ and $CeO_2-TiO_2$ catalyst systems, Larsson and Andersson[6] concluded that the distribution of copper species depended on both copper oxide and ceria loading. Moreover, they observed the presence of bulk CuO crystallites in both systems only in higher copper-loaded samples.[4,6]

**HR-TEM Micrographs.** Figure 2 shows the micrographs of several samples ($TiO_2$, $Ti_{0.91}O_{1.82}Cu_{0.09}$, $Ce_{0.09}Ti_{0.82}O_{1.91}Cu_{0.09}$, and $Ce_{0.45}Ti_{0.46}O_{1.91}Cu_{0.09}$). The fringes appearing in the micrographs allow for the identification of the crystallographic spacing of the $TiO_2$ and $CeO_2$ nanocrystallites that are identified

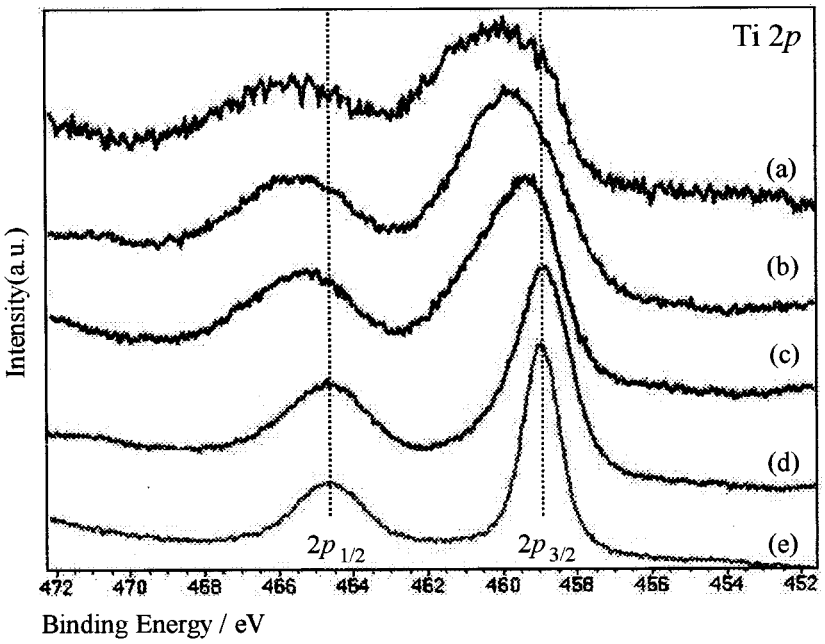


**Figure 3.** Ti 2p XP spectra of (a) $Ce_{0.45}Ti_{0.46}O_{1.91}Cu_{0.09}$, (b) $Ce_{0.27}Ti_{0.64}O_{1.91}Cu_{0.09}$, (c) $Ce_{0.09}Ti_{0.82}O_{1.91}Cu_{0.09}$, (d) $Ti_{0.91}O_{1.91}Cu_{0.09}$ catalysis, and (e) $TiO_2$−anatase reference.

in the micrographs. The fringes most frequently observed correspond respectively to the (101) and (111) crystallographic planes of $TiO_2$ anatase and $CeO_2$ cerianite phases.

Only the fringes assigned to $TiO_2$ anatase and $CeO_2$ cerianite phases were observed, confirming our previous statement about a well-dispersed copper species on the support, which was revealed by Raman analysis and XRD data.[15]

Although the $CeO_2$ crystallites was also observed in the micrographs, only the $TiO_2$ average crystallites sizes were measured (see Table 1). The HR-TEM micrographs show a significant increase of titania crystallite sizes ranging from 5 to 17 nm. The samples without $CeO_2$, ($TiO_2$ in Figure 2a and $Ti_{0.91}O_{1.82}Cu_{0.09}$ in Figure 2b) presented the same crystallite sizes, indicating that copper oxide caused no modification in $TiO_2$ anatase crystallite size. The $TiO_2$ particle size decreased as the amount of $CeO_2$ on the support increased (Figure 2c,d). Previous XRD measurements also revealed a trend toward smaller $TiO_2$ crystallites with the addition of $CeO_2$ to the support.[15]

HR-TEM micrographs and textural analyses, therefore, showed that the $Ce_{0.09}Ti_{0.82}O_{1.91}Cu_{0.09}$ catalyst presented a higher surface area and a smaller titania crystallite size than the samples without $CeO_2$ ($TiO_2$ and $Ti_{0.91}O_{1.91}Cu_{0.09}$). Otherwise, there was a reduction of both surface area and titania particle size in the samples with higher amounts of $CeO_2$. This fact was attributed to the formation of isolated $CeO_2$ particles, which presented a very small surface area (25 $m^2/g$), thus contributing toward the decrease in the total surface area of the catalysts.

**XP Spectroscopic Analysis.** The binding energy values of the main peaks in the XPS of reference and catalysts are summarized in Table 2.

Figure 3 shows the Ti 2p XP spectra of the catalysts and $TiO_2$−anatase. The spin−orbit components ($2p_{3/2}$ and $2p_{1/2}$) of each peak of the $TiO_2$ and $Ti_{0.91}O_{1.91}Cu_{0.09}$ spectra were well deconvoluted by two curves (at approximately 459.0 and 464.6 eV, respectively) corresponding to $Ti^{4+}$ in a tetragonal structure.[23] Otherwise, the XP spectra of samples containing $CeO_2$ were better fitted considering the presence of a second $Ti^{4+}$ species. The peak assigned to this second $Ti^{4+}$ species had

**TABLE 2: XPS Binding Energy Values as a Function of $CeO_2$ Content for the References and Samples**

| | B. E. eV | | | | |
|---|---|---|---|---|---|
| | Cu | Ti | Ce | O 1*s* | |
| samples | $2p_{3/2}$ | $2p_{3/2}$ | $3d_{5/2}$ | $OH^-$ | $O_{lattice}$ |
| $CeO_2$ | | | 882.7 | 531.7 | 529.4 |
| $TiO_2$ | | 459.0 | | 531.7 | 530.1 |
| $Ce_{0.91}O_{1.91}Cu_{0.09}$ | 933.7 | | 882.3 | 531.4 | 529.4 |
| $Ti_{0.91}O_{1.91}Cu_{0.09}$ | 933.7 | 459.0 | | 531.4 | 529.4 |
| $Ce_{0.09}Ti_{0.82}O_{1.91}Cu_{0.09}$ | 933.6 | 459.2/460.8 | 883.2 | 532.1 | 530.5 |
| $Ce_{0.27}Ti_{0.64}O_{1.91}Cu_{0.09}$ | 933.7 | 429.3/460.6 | 882.6 | 531.5 | 530.0 |
| $Ce_{0.45}Ti_{0.46}O_{1.91}Cu_{0.09}$ | 933.8 | 458.7/460.5 | 882.2 | 531.6 | 529.9 |
| CuO | 933.9 | | | 531.8 | 529.9 |
| $Cu_2O$ | 932.1 | | | 531.9 | 530.2 |

shifted to a higher energy ($2p_{3/2}$ peak at 459.2 eV) and intensified with the addition of $CeO_2$.

Alves et al.[24] obtained XPS results similar to ours for $IrO_2$−$TiO_2$−$CeO_2$ electrocatalysts. The Ti 2p spectra became larger and shifted to higher energy values in $CeO_2$ rich samples, leading them to suggest that this element is present in more than one species. The XPS analysis of these authors revealed a strong interaction between $TiO_2$ and $SiO_2$.[25] They also observed an upward shift of the Ti 2p XP-spectra in this system, which they ascribed to an increase in the interatomic potentials due to a decrease of the coordination number of Ti and shortening of the Ti−O bond.

Our XPS results indicate the presence of a second $Ti^{4+}$ species on the sample surface as the amount of $CeO_2$ increased, which is corroborated by our previous Ti K-edge XANES analysis.[15]

Figure 4 shows the Ce 3d XP spectra, and Figure 5 displays a curve fitting example of the Ce 3d XPS peaks ($Ce_{0.45}Ti_{0.46}O_{1.91}$-$Cu_{0.09}$ sample). The ground state of $CeO_2$ is a mixture of multielectron configurations $4f^0$ and $4f^1L$, where $L$ denotes a hole in the oxygen 2p orbitals (ligand hole), whereas the ground state of $Ce_2O_3$ is purely $4f^1$.[26] The Ce 3d photoemission gives rise to a rearrange of valance electrons. The XPS Ce $3d_{5/2}$ and $3d_{3/2}$ doublets are commonly denoted $u$ and $v$ and extend in the energy range of 880−920 eV.[6,20,26,27] For $CeO_2$, the final states due to the photoemission of the Ce 3d give rise to six peaks ascribed to the three pairs of the spin−orbita doublets ($3d_{5/2}$ e

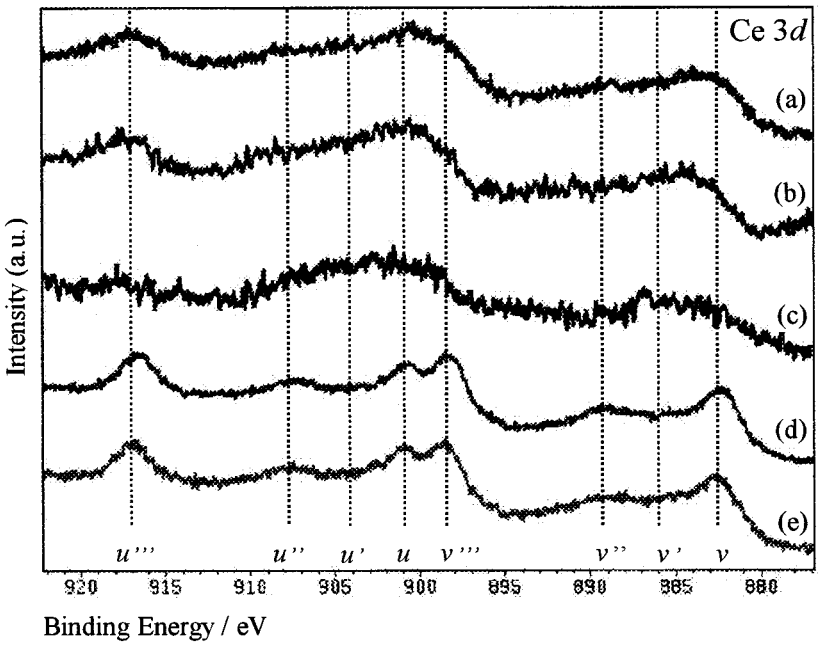


**Figure 4.** Ce 3d XP spectra of (a) $Ce_{0.45}Ti_{0.46}O_{1.91}Cu_{0.09}$, (b) $Ce_{0.27}Ti_{0.64}O_{1.91}Cu_{0.09}$, (c) $Ce_{0.09}Ti_{0.82}O_{1.91}Cu_{0.09}$, (d) $Ce_{0.91}O_{1.91}Cu_{0.09}$ catalysis, and (e) $CeO_2$ reference.

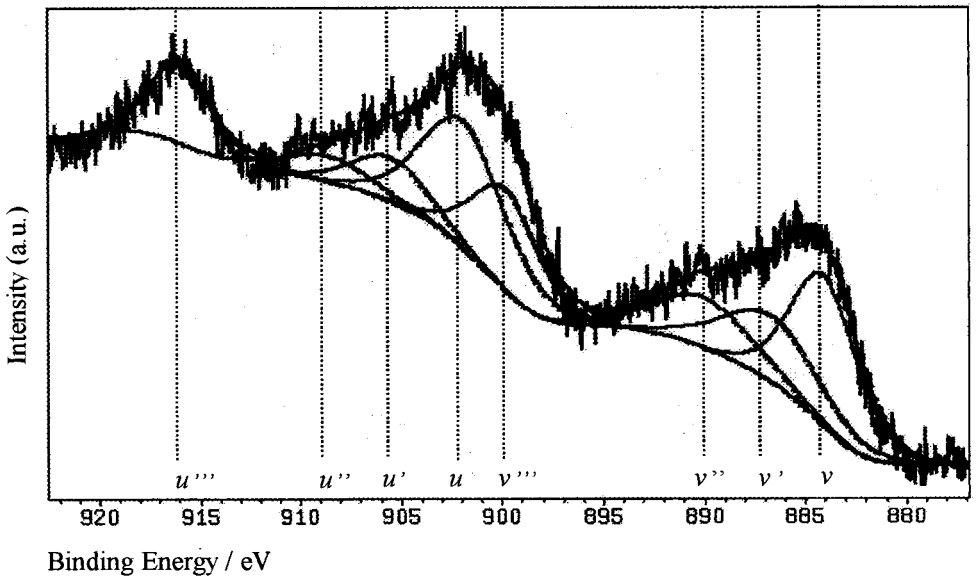


**Figure 5.** Fitting of the Ce 3d XP spectrum obtained from the $Ce_{0.45}Ti_{0.46}O_{1.91}Cu_{0.09}$ catalysis.

$3d_{3/2}$). These six peaks are due to the different ways of occupancy of the Ce 4f final state strongly hybridized with the oxygen 2p orbital. The $v$ and $v''$ peaks are attributed to the bonding and antibonding states arising from the multielectron configuration $3d^94f^2(O\ 2p^4)$ and $3d^94f^1(O\ 2p^5)$ $Ce^{4+}$, and the $v'''$ peak to a $3d^94f^0(O\ 2p^6)$ $Ce^{4+}$ final state.[6,13,20,26,27] In the case of $Ce_2O_5$, the Ce 3d photoemission lines correspond to two pairs of spin−orbital doublets ($3d_{5/2}$ e $3d_{3/2}$), which arise from the hybridization of the multielectron configurations $4f^1$ and $4f^2$. However, one of the pairs (denoted $u_0$ and $v_0$) is hardly observed because it is a shoulder on the $Ce^{4+}$ 3d spectrum. The $v'$ peak corresponds to the $3d^94f^1(O\ 2p^6)$ $Ce^{3+}$ final state.[6,13,20,27] The same explanation holds true for the series of $u$ structures of the $3d_{3/2}$ level.

After the deconvolution of the Ce 3d spectra, the degree of reduction ($Ce^{3+}$ species) can be estimated from the intensity of $v'$ and $u'$ lines, according to the following equation:[6,13,28,29]

$$Ce^{3+}(\%) = \frac{S_{v'} + S_{u'}}{\sum(S_v + S_u)}100$$

where $S_{v'}$ and $S_{u'}$ are the intensities of $v'$and $u'$ lines and $S_v$ and $S_u$ are the intensities of $v$ and $u$ lines.

Table 3 shows the amount of $Ce^{3+}$ calculated for $CeO_2$ and the catalysts. As can be observed, even for the $CeO_2$ sample, the percentage of Ce reduction is equal to 15%, a similar value calculated for the $Ce_{0.91}O_{1.91}Cu_{0.09}$ catalyst. The $Ce_{0.09}Ti_{0.82}O_{1.91}$-$Cu_{0.09}$ catalyst presents the highest percentage of surface $Ce^{3+}$ species, 27%. For the others samples, the reduction of ceria also took place but in a smaller proportion. The reduction of cerium ions during XPS measurements has been reported in the literature [6,8,28,30−32] and must be taken into account when

**TABLE 3: Estimation of the $Ce^{3+}$(%) Amount Calculated from the Ce 3d Peaks and the Atomic Ratios as a Function of Ce Content for References and Samples[a]**

| | | atomic ratio | | |
|---|---|---|---|---|
| samples | $Ce^{3+}$(%) | Ce/Ti | Cu/Ce | Cu/Ti |
| $CeO_2$ | 0.14 | | | |
| $Ce_{0.91}O_{1.91}Cu_{0.09}$ | 0.15 | | 0.17 | |
| $Ti_{0.91}O_{1.91}Cu_{0.09}$ | | | | 0.14 |
| $Ce_{0.09}Ti_{0.82}O_{1.91}Cu_{0.09}$ | 0.27 | 0.10 | 1.91 | 0.19 |
| $Ce_{0.27}Ti_{0.64}O_{1.91}Cu_{0.09}$ | 0.20 | 0.33 | 0.60 | 0.20 |
| $Ce_{0.45}Ti_{0.46}O_{1.91}Cu_{0.09}$ | 0.22 | 0.64 | 0.41 | 0.26 |

[a] The experimental error was estimated as approximately 15%.

discussing about the oxidation state of surface species. According to some XPS time-dependent studies,[6,30] the reduction takes place during the first minutes of measurements. Park et al.[31] found that amorphous cerium oxide is reduced more extensively than the crystalline form during XPS analysis. The reduction of $Ce^{4+}$ ions by X-ray exposition in the $TiO_2/CeO_2$ mixed support prepared by sol−gel method occurred more effectively than the physical mixture of the two oxides.[32]

We performed a time-dependent XPS experiment in order to verify if the above-mentioned effect also occurred for our samples. New features appeared in the Ce 3d spectrum as the time of measurement increased, indicating a photoreduction effect. The samples containing lower amount of ceria presented higher photoreduction because of the longer acquisition time required to improve the signal-to-noise ratio (Table 3). On the basis of these observations, we infer that the cerium species present in the catalyst samples are in the $Ce^{4+}$ state. Our previous EXAFS results corroborated by this conclusion.[15]

Figure 6 presents the Cu 2p XPS results. The Cu 2p XP spectrum of CuO was easily identified by the $2p_{3/2}$ main peak at 934.2 eV and the satellite at about 940−945 eV.[7] In the case of the catalyst spectra, the Cu $2p_{3/2}$ components were positioned very close to each other at 933.8 eV. The catalysts presented a weak satellite owing to their lower amount of copper (9% in atomic units). The copper species of all of the catalysts were dispersed as $Cu^{2+}$, an, as discussed previously, no peak was ascribed to any copper phase in the diffraction pattern[16] and no copper band was identified by Raman measurements.

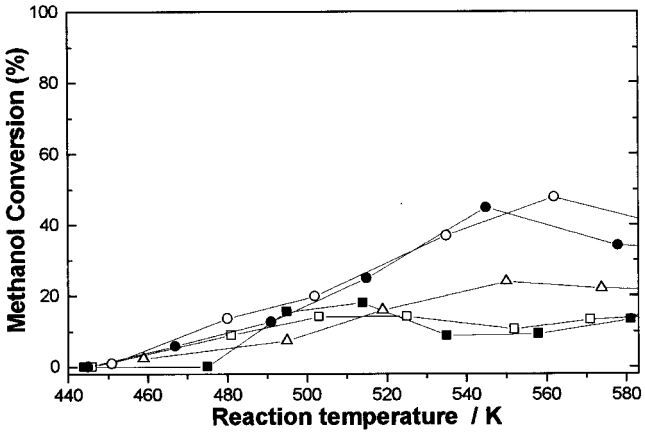


**Figure 7.** Catalytic activity of $Ce_{0.45}Ti_{0.46}O_{1.91}Cu_{0.09}$ (△), $Ce_{0.27}Ti_{0.64}O_{1.91}Cu_{0.09}$ (○), $Ce_{0.09}Ti_{0.82}O_{1.91}Cu_{0.09}$ (●), $Ti_{0.91}O_{1.91}Cu_{0.09}$ (■), $Ce_{0.91}O_{1.91}Cu_{0.09}$ (□) for the totalmethanol conversion as a function of the reaction temperature.

The Ce/Ti, Cu/Ce, and Cu/Ti surface atomic ratios are also presented in Table 3. Taking into account the XPS quantitative resolution, the measured Ce/Ti ratios for the $Ce_{0.09}Ti_{0.82}O_{1.91}Cu_{0.09}$ and $Ce_{0.27}Ti_{0.64}O_{1.91}Cu_{0.09}$ catalysts are approximately equal to the nominal values. Concerning the $Ce_{0.45}Ti_{0.46}O_{1.91}Cu_{0.09}$ sample, the Ce/Ti ratio is 36% lower than its nominal composition. This result can be explained by the fact that this composition presents the higher amount of $CeO_2$ phase.

Concerning the Cu/Ce atomic ratio, as expected, the Cu/Ce atomic ratio decreases as the amount of Ce increases. Comparing these values with their nominal compositions, we observed that they are approximately two times higher, indicating that copper atoms are really dispersed on the catalysts surface. This supposition is also supported by the Cu/Ti atomic ratio values, which increases with cerium loading and presents a higher value when compared to their respective nominal compositions.

**Methanol Oxidation.** Figure 7 shows the catalytic properties of the $CuO/TiO_2$, $CuO/CeO_2$, and $CuO-CeO_2/TiO_2$ catalysts for total methanol conversion as a function of the reaction temperature. All of the catalysts exhibited methanol dehydrogenation activity at temperatures above 463 K. The catalysts

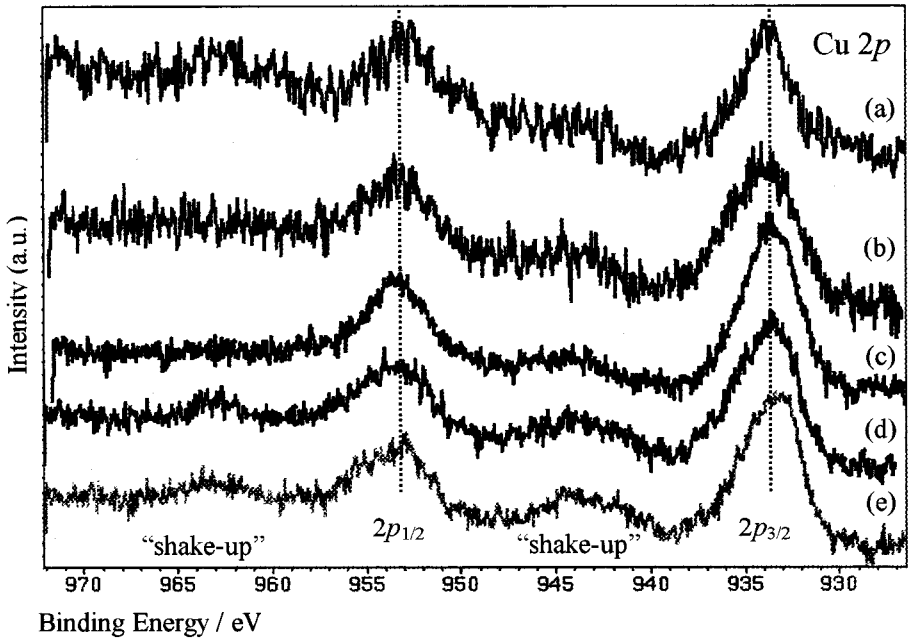


**Figure 6.** Cu 2p XP spectra of (a) Ce0.91O1.91Cu0.09, (b) $Ce_{0.45}Ti_{0.46}O_{1.91}Cu_{0.09}$, (c) $Ce_{0.27}Ti_{0.64}O_{1.91}Cu_{0.09}$, (d) $Ce_{0.09}Ti_{0.82}O_{1.91}Cu_{0.09}$, and (e) $Ti_{0.91}O_{1.91}Cu_{0.09}$ catalysis.

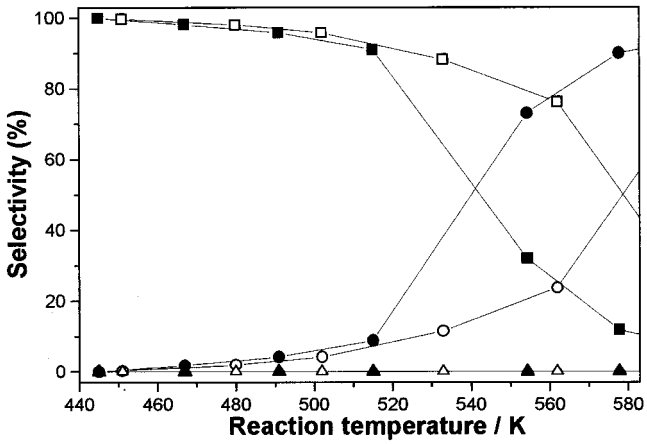


**Figure 8.** Effect of reaction temperature on selectivity over $Ce_{0.09}Ti_{0.82}O_{1.91}Cu_{0.09}$ (closed symbols) and $Ce_{0.27}Ti_{0.64}O_{1.91}Cu_{0.09}$ (open symbols) catalysis to methyl formate (■/□), formaldehyde (●/○), and $CO_x$ (□/△).

containing 9 and 27% of $CeO_2$ presented the highest methanol conversion (approximately 44%) at around 555 K, whereas the $Ti_{0.91}O_{1.91}Cu_{0.09}$ reached a conversion of 22% at approximately 514 K.

These results show that the ceria-modified $TiO_2$ support in combination with the presence of CuO promoted greater methanol conversion than the catalyst using a pure $TiO_2$ support ($Ti_{0.91}O_{1,91}Cu_{0,09}$ sample), indicating a synergistic effect between Cu and the $CeO_2-TiO_2$ support.

Our observations are in general agreement with those of other authors. Liu and Flytzani-Stephanopoulos[9,10] studied the Cu−Ce−O system, concluding that, in samples containing smaller amounts of copper, this element is finely dispersed on ceria and that the synergistic effect between CuO and $CeO_2$ produces highly active sites for CO and methane combustion. A TPR investigation of a $CuO/CeO_2$ catalyst showed that $CeO_2$ promotes the reduction of CuO species at low temperatures and that these species are finely dispersed on the ceria surface.[11]

Figure 8 illustrates the effect of the reaction temperature on the selectivity over the $Ce_{0.09}Ti_{0.82}O_{1.91}Cu_{0.09}$ and $Ce_{0.27}Ti_{0.64}O_{1.91}Cu_{0.09}$ catalysts to methyl formate (MF), formaldehyde (F), and $CO_x$. The results indicated that both catalysts show a high selectivity for MF at low reaction temperatures. The methanol in the $Ce_{0.27}Ti_{0.64}O_{1.91}Cu_{0.09}$ sample was converted into MF with maximum selectivity in the range of 443−583 K. Even at a high temperature (579 K), the selectivity for MF was 50%. In contrast, for the $Ce_{0.09}Ti_{0.82}O_{1.91}Cu_{0.09}$ catalyst, the maximum selectivity for MF lay in the range of 443−513 K, and an MF selectivity of 50% was obtained at 541 K. Methanol conversion into $CO_x$ was negligible in both catalysts, regardless of the reaction temperature.

On the basis of the structural results presented in this paper, the following structural model for the catalyst samples is proposed: in samples containing a low amount of $CeO_2$ (9%), a cerium surface layer is apparently formed on the titania particles. In this situation, copper species are well dispersed on the particles and the catalysts present maximum methanol conversion. This assumption is well supported by the XPS results, which showed a second Ti atom species in a distorted structure after the addition of ceria. Moreover, the EXAFS measurements at the Ce $L_{III}$-edge also revealed that, in sample catalysts containing 9% of ceria, the cerium atoms presented a well distorted local structure, which could also indicate an interaction between Ce, Ti, and Cu atoms.[15]

As the amount of ceria increased (27 and 45% of $CeO_2$), the catalytic performance decreased. This decrease may be explained by the formation of isolated $CeO_2$ particles. In this case, copper atoms are also dispersed in the isolated $CeO_2$ particles, interacting only with Ce atoms. This supposition was supported first by the BET surface area measurements, which showed a reduction of the surface area in samples containing more than 9% of ceria. Second, our Raman results clearly showed the presence of a peak around 450 $cm^{-1}$ assigned to the $CeO_2$ phase, whereas $CeO_2$ particles were only observed by TEM in samples containing more than 27% of cerium. Furthermore, previous XRD and Ce $L_{III}$ XAS analyses also revealed the presence of isolated $CeO_2$ particles in samples containing more than 9% of ceria.[16]

To summarize, our above-discussed results indicated that, in the samples containing the lower amount of $CeO_2$ ($Ce_{0.09}Ti_{0.82}O_{1.91}Cu_{0.09}$ catalyst), the $CeO_2$ formed a surface layer on the titania particle and that, in this situation, copper atoms interact with Ce and Ti atoms. As the amount of ceria increases, a formation of isolated $CeO_2$ particles is observed, and some of the copper atoms may interact with this isolated phase, decreasing the catalytic activity in the samples.

## Conclusions

A small addition of $CeO_2$ to the $CuO/TiO_2$ system increased the specific surface area of the catalyst. Using a larger amount of $CeO_2$, the surface areas decreased, probably because of ceria segregation, contributing to the reduction of the total surface area.

Only two types of crystalline phases were observed by Raman and TEM micrography: $TiO_2$ anatase and $CeO_2$ cerianite. No CuO phases were detected, indicating that copper species were well dispersed on the support. TEM micrographs of the catalysts showed a trend toward smaller $TiO_2$ crystallites as $CeO_2$ was added to the support, which explains the greater overall surface area of the samples containing a small amount of $CeO_2$.

An XPS surface analysis indicated that titanium from $CuO/CeO_2-TiO_2$ catalysts showed the presence of a second titanium $Ti^{4+}$ species, which increases with the addition of cerium, and that the samples containing cerium apparently have part of this element as $Ce^{3+}$. The XPS data also revealed that the copper species was dispersed on the support in the form of $Cu^{2+}$.

The catalysts containing a minor amount of $CeO_2$ presented the highest methanol conversion owing to the synergistic effect between copper and the $CeO_2-TiO_2$ support. In the catalyst samples containing higher amounts of $CeO_2$, the presence of $CeO_2$ as a major crystalline phase may have been responsible for the reduced catalytic activity. Copper supported on the mixed oxides appears to have a better catalytic performance than copper supported on $CeO_2$ or $TiO_2$.

**Acknowledgment.** This work was supported by the Brazilian research funding institutions FAPESP and CNPq. The research work was performed partially at the Laboratório de Microscopia Eletrônica (LME) of the National Synchrotron Light Laboratory and partially at the Grupo de Propriedades Ópticas (GPO) of the IFGW-UNICAMP, Brazil.

## References and Notes

(1) Takezawa, N.; Iwasa, N. *Catal. Today* **1997**, *36*, 45.
(2) Breen, J. P.; Ross, J. R. H. *Catal. Today* **1999**, *51*, 521.
(3) Dong, G.; Wang, J.; Gao, Y.; Chen, S. *Catal. Lett.* **1999**, *58*, 37.
(4) Larsson, P.-O.; Andersson, A. *Appl. Catal. B* **2000**, *24*, 175.
(5) Kumar, P. M.; Badrinarayanan, S.; Sastry, M. *Thin Solid Films* **2000**, *358*, 122.

(6) Larsson, P.-O.; Andersson, A. *J. Catal.* **1998**, *179*, 72.
(7) Guerrero-Ruiz, A.; Rodriguez-Ramos, I.; Fierro, J. L. G. *Appl. Catal.* **1991**, *72*, 119.
(8) Trovarelli, A.; Zamar, F.; Lorca, J.; Leitenburg, C.; Kiss, J. T. *J. Catal.* **1997**, *169*, 490.
(9) Liu, W.; Flytzani-Stephanopoulos, M. *J. Catal.* **1995**, *153*, 304.
(10) Liu, W.; Flytzani-Stephanopoulos, M. *J. Catal.* **1995**, *153*, 317.
(11) Luo, M.-F.; Zhong, Y.-J.; Yuan, X.-X.; Zheng, X.-M. *Appl. Catal. B* **1997**, *162*, 121.
(12) Alves, V. A.; Silva, L. A.; Castro, S. C.; Boodts, F. C. *J. Chem. Soc., Faraday Trans.* **1998**, *94*, 711.
(13) Ernst, B.; Hilaire, L.; Kiennemann, A. *Catal. Today* **1999**, *50*, 413.
(14) Tatibouët, J. M. *Appl. Catal. A* **1997**, *148*, 213.
(15) Francisco, M. S. P.; Nascente, P. A. P.; Mastelaro, V. R.; Florentino, A. O. *J. Vac. Sci. Technol. A* **2001**, *19*, AIP ID# 042104JVA.
(16) Yuan, S.; Mériaudeau, P.; Perrichon, V. *Appl. Catal. B* **1994**, *3*, 319.
(17) Kosuge, K.; Singh, P. S. *J. Phys. Chem. B* **1999**, *103*, 3563.
(18) Davis, R. J.; Liu, Z. *Chem. Mater.* **1997**, *9*, 2311.
(19) Busca, G.; Ramis, G.; Amores, J. M. G. V.; Escribano, S.; Piaggio, P. *J. Chem. Soc., Faraday Trans.* **1994**, *90*, 3181.
(20) Shyu, J. Z.; Weber, W. H.; Gandhi, H. S. *J. Phys. Chem.* **1988**, *92*, 2, 17.
(21) Reimann, K.; Syassen, K. *Solid State Commun.* **1990**, *76*, 137.
(22) Gonzalez, R. D.; Lopez, T.; Gomez, R. *Catal. Today* **1997**, *35*, 293.
(23) Lu, L.; Bernasek, S. L.; Schwartz, J. *Surf. Sci.* **2000**, *458*, 80.
(24) Alves, V. A.; Silva, L. A.; Boodts, F. C. *Química Nova* **2000**, *23*, 608.
(25) Stakheev, A. Y.; Shapiro, E. S.; Apijok, J. *J. Phys. Chem.* **1993**, *97*, 5668.
(26) Thromat, N.; Gautier-Soyer, M.; Bordier, G. *Surf. Sci.* **1996**, *345*, 290.
(27) Normand, F. L.; Hilaire, L.; Kili, K.; Krill, G.; Maire, G. *J. Phys. Chem*, **1988**, *92*, 2561.
(28) Daturi, M.; Binet, C.; Lavalley, J.-C.; Galtayries, A.; Sporken, R. *Phys. Chem. Chem Phys.* **1999**, *1*, 5717.
(29) Laachir, A.; Perrichon, V.; Badri, A.; Lamotte, J.; Catherine, E.; Lavalley, J. C.; Fallah, J. E.; Hilaire, L.; Normand, F. I.; Quéméré, E.; Sauvion, G. N.; Touret, O. *J. Chem. Soc., Faraday Trans.* **1991**, *87*, 1601.
(30) Galtayries, A.; Sporken, R.; Riga, J.; Blanchard, G.; Caudano, R. *J. Electron Spectrosc. Relat. Phenom.* **1998**, *88*, 951.
(31) Park, W. P.; Ledford, J. S. *Langmuir* **1996**, *12*, 1794.
(32) Dauscher, A.; Wehrer.; Hilaire, L. *Catal. Lett.* **1992**, *14*, 171.